JACS
JOURNAL OF THE AMERICAN CHEMICAL SOCIETY

Communication

A Three-Dimensional Lead Halide Perovskite-Related Ferroelectric

Han-Yue Zhang, Xian-Jiang Song, Hao Cheng, Yu-Ling Zeng,
Yi Zhang, Peng-Fei Li, Wei-Qiang Liao, and Ren-Gen Xiong

J. Am. Chem. Soc., **Just Accepted Manuscript** • DOI: 10.1021/jacs.0c00375 • Publication Date (Web): 23 Feb 2020

is published by the American Chemical Society. 1155 Sixteenth Street N.W., Washington, DC 20036

A Three-Dimensional Lead Halide Perovskite-Related Ferroelectric

Han-Yue Zhang,[†] Xian-Jiang Song,[†] Hao Cheng,[§] Yu-Ling Zeng,[§] Yi Zhang,[†] Peng-Fei Li,[§] Wei-Qiang Liao,[§] and Ren-Gen Xiong*,[†,§]

[†]Jiangsu Key Laboratory for Science and Applications of Molecular Ferroelectrics, Southeast University, Nanjing 211189, People's Republic of China

[§]Ordered Matter Science Research Center, Nanchang University, Nanchang 330031, People's Republic of China

Supporting Information Placeholder

ABSTRACT: Three-dimensional (3D) organic-inorganic lead halides represented by $[CH_3NH_3]PbI_3$ perovskite have attracted great interest for their diverse functional properties and promising optoelectronic applications. However, 3D lead halides are still very rare and their ferroelectricity remains controversial. Here, we report an unprecedented 3D lead halide perovskite-related ferroelectric [2-trimethylammonioethylammonium]Pb_2Cl_6 ([TMAEA]Pb_2Cl_6), which contains a 3D lead chloride framework of corner- and edge-sharing $PbCl_6$ octahedral, with the $[TMAEA]^+$ cations occupying the voids of the framework. [TMAEA]Pb_2Cl_6 shows a ferroelectric-to-paraelectric phase transition with the Curie temperature as high as 412 K, a typical ferroelectric hysteresis loop at 293 K with a spontaneous polarization of 1 μC/cm^2, and a clear ferroelectric domain switching. To the best of our knowledge, [TMAEA]Pb_2Cl_6 is the first 3D lead halide showing such an excellent ferroelectricity. Additionally, it also exhibits semiconducting property with a direct bandgap of 3.43 eV. This finding enriches the family of 3D hybrid lead halides, and inspires the exploration of 3D lead halide ferroelectrics.

Organic-inorganic lead halides (OILHs) with perovskite or perovskite-related crystal structures have gained worldwide attention in recent years as promising semiconductors for applications in solar cells, smart photovoltaic windows, photodetectors, light emitting diodes, etc.[1,2] Among them, the three-dimensional (3D) $APbX_3$ (A = organic cation, X = Cl, Br, I) perovskites are particularly attractive because of their unique 3D structures and superior optoelectronic properties.[2] $APbX_3$ adopts the cubic perovskite structure, which is composed of a 3D lead halide framework of corner-sharing PbX_6 octahedra, with A cations residing in the holes formed by adjacent PbX_6 octahedra.[3] To obey the Goldschmidt tolerance factor rule, the A cation is limited to the small size $[CH_3NH_3]^+$ and $[NH_2(CH)NH_2]^+$ cations.[4] Great efforts have been made to extend the family of 3D OILHs, however, 3D OILHs still remain very sparse.[3,5] Organic-inorganic hybrid crystal structures derived from perovskite are rich,[6] and the connectivity of the PbX_6 octahedra is diverse, varying from corner-sharing to face-sharing to edge-sharing,[3] but most of OILHs are of the zero-, one- or two-dimensional structure.[3] Discovering a new 3D OILHs is a great challenge.

Besides semiconductors, structurally, the free motion of organic cation in the space enclosed by the PbX_6 octahedra makes OILHs candidates for ferroelectrics,[7] which possess spontaneous polarization (P_s) and are able to switch the Ps under an external electric filed.[8] The P_s can induce a built-in electric field, facilitating the separation of photoexcited carriers.[9] This unique feature results in some extraordinary optoelectronic phenomena in ferroelectric semiconductors, such as the switchable photovoltaic effects and large photovoltage in $BiFeO_3$.[10] Researchers also deemed that the possible ferroelectricity in 3D $[CH_3NH_3]PbI_3$ contributed to its outstanding photovoltaic performance.[11] Combined with the ferroelectricity, semiconducting property, and the advantages of low cost, easy processing, and mechanical flexibility within a single molecular compound, the organic-inorganic lead halide ferroelectric semiconductors (OLHFS) are promising for next-generation optoelectronic devices.[12] In this context, some one-dimensional (1D) and two-dimensional (2D) OILHs were recently discovered as OLHFS,[7,12,13] such as the 1D $[(CH_3)_3NCH_2I]PbI_3$[13a] and the 2D (benzylammonium)$_2PbCl_4$,[7a] [cyclohexylammonium]$PbBr_4$,[7b] [4,4-diflorocyclohexylammonium]$_2PbI_4$,[13b] [2-fluorobenzylammonium]$_2PbCl_4$,[13c] [ethylammonium]$_4Pb_3Br_{10}$,[13d] [4-aminotetrahydropyran]$_2PbBr_4$,[13e] and [*R*-1-(4-chlorophenyl)ethylammonium]$_2PbI_4$.[13f] Nevertheless, whether the 3D $[CH_3NH_3]PbI_3$ has ferroelectricity or not is still under debate due to the lack of convinced evidence to prove its ferroelectricity.[14] And the centrosymmetric *Pm3m* space group in $[CH_3NH_3]PbCl_3$ and $[CH_3NH_3]PbBr_3$ fails to meet the polar symmetry for ferroelectrics.[15] To date, genuine 3D OLHFS are still not documented, though ferroelectricity have been found in other 3D organic-inorganic hybrids,[16] such as the metal-formate $[NH_4][M(HCOO)_3]$ (M = Mn, Fe, Co, Ni, Zn),[16a] the alkali-metal halide perovskite [3-ammoniopyrrolidinium]$RbBr_3$,[16c] and the metal-free perovskite [*N*-methyl-*N*′-diazabicyclo[2.2.2]octonium]NH_4I_3.[16d]

Here, we find that [2-trimethylammonioethylammonium]Pb_2Cl_6 ([TMAEA]Pb_2Cl_6), which adopts a 3D perovskite-related structure consisting of a 3D lead chloride framework of corner- and edge-sharing $PbCl_6$ octahedral, shows a clear ferroelectricity with a high Curie temperature of 412 K and a spontaneous polarization of 1 μC/cm^2 and semiconducting property with a direct bandgap of 3.43 eV. As far as we know, [TMAEA]Pb_2Cl_6 is the first example of 3D OLHFS. This finding opens up possibilities for exploring new 3D organic-inorganic lead halides, especially the 3D lead halide ferroelectric semiconductors.

[TMAEA]Pb_2Cl_6 was prepared by reacting stoichiometric amounts of the synthesized [TMAEA]Cl_2 and the $PbCl_2$ in the concentrated hydrochloric acid. We used the powder X-ray diffraction determination to confirm the phase purity of [TMAEA]Cl_2 and [TMAEA]Pb_2Cl_6 (Figures S1 and S2), and the thermogravimetric analysis to show the thermal stability of [TMAEA]Pb_2Cl_6 up to about 580 K (Figure S3). [TMAEA]Pb_2Cl_6 crystallizes in the orthorhombic polar space group *Pma*2 (point

group *mm*2 (C_{2v})) at 293 K (room-temperature phase, RTP) (Table S1), different from the cubic centrosymmetric *Pm*3*m* one in $[CH_3NH_3]PbCl_3$.[15] The crystal structure of $[TMAEA]Pb_2Cl_6$ contains 3D lead-chloride inorganic frameworks of corner- and edge-sharing $PbCl_6$ octahedral, of which the voids are occupied by the $[TMAEA]^+$ organic cations, adopting an organic-inorganic perovskite-related structure (Figure 1).[17] In the $PbCl_6$ octahedron, the Pb center is coordinated by six bridging Cl atoms with Cl–Pb–Cl bond angles of 81.6(3)–176.2(4)° (Table S2), showing a distorted coordination geometry. The $PbCl_6$ octahedron connects with an adjacent one through the edge-sharing mode to form a $[Pb_2Cl_6]^{2-}$ dimer, which further links with adjacent dimers through the corner-sharing mode to form a 3D network (Figure S4). OILHs featuring both edge- and corner-sharing modes are rare, though it was also found in the 1D lead-bromide perovskite-related $(C_6H_{16}N_2)_3Pb_2Br_{10}$ and the 2D one $(C_5H_{14}N_2)_2Pb_3Br_{10}$.[17] Each cavity of the 3D network in $[TMAEA]Pb_2Cl_6$ are composed of twelve $PbCl_6$ octahedral, which are large enough to accommodate the $[TMAEA]^+$ cations (Figure 1a). Between the anionic framework and $[TMAEA]^+$ cations, there are weak N–H···Cl hydrogen-bonding interactions with an average N···Cl distance of 3.291 Å (Figure S5a). The $[TMAEA]^+$ cation lies on a symmetry position of the mirror plane parallel to the *bc* plane, and shows a two-fold orientational disorder (Figure S5b). As Figure 1c shows, the polar $[TMAEA]^+$ cations are arranged in the *c*-axis with one orientation, which will results in a spontaneous polarization.

Differential scanning calorimetry (DSC) analysis reflects that $[TMAEA]Pb_2Cl_6$ experiences two phase transitions at around T_1 = 361 K and T_2 = 412 K, respectively (Figure 2a). We thus further determined the crystal structure of $[TMAEA]Pb_2Cl_6$ at 393 K in the intermediate-temperate phase (ITP) and at 423 in the high-temperature phase (HTP). In ITP, $[TMAEA]Pb_2Cl_6$ has the same *Pma*2 space group as in RTP (Table S1), and both the 3D anionic framework and $[TMAEA]^+$ cations show no obvious change from RTP to ITP (Table S2 and Figure S5), which indicates that the phase transition at T_1 is an isostructural one. However, in HTP, the space group of $[TMAEA]Pb_2Cl_6$ becomes the orthorhombic centrosymmetric *Pmma* (point group *mmm* (D_{2h})) (Table S1). The Pb–Cl bond distances and Cl–Pb–Cl bond angles of $PbCl_6$ octahedron are comparable to those in ITP (Table S2). While the $[TMAEA]^+$ cation becomes four-fold orientationally disordered, since its symmetry positon changes to two mirror plane parallel to the *bc* and *ac* plane, respectively (Figure S5d). The orientations of the $[TMAEA]^+$ cation are related by the mirror plane (Figure 1d), leading to the offset of dipolar moments. The phase transition at T_2 can thus be ascribed to the orientation change of $[TMAEA]^+$ cations.

Real part (ε') of the dielectric permittivity of $[TMAEA]Pb_2Cl_6$ presents a remarkable anomaly near T_2 (Figure 2b), further verifying the phase transition at T_2. No obvious dielectric anomaly was observed during the phase transition at T_1, maybe due to its isostructural nature. We also employed the second harmonic generation (SHG) experiment to investigate the phase transition (Figure 2c). $[TMAEA]Pb_2Cl_6$ displays a clear SHG signal with the intensity about one fifth of that of KH_2PO_4 (KDP) at 293 K, according with the polar *Pma*2 space group. As temperature increases, the SHG intensity weakens gradually, and reduces to zero near T_2. This manifests that the phases below and above T_2 are non-centrosymmetric and centrosymmetric ones, respectively, corresponding to the polar *Pma*2 space group in RTP and ITP and the centrosymmetric *Pmma* space group in HTP.

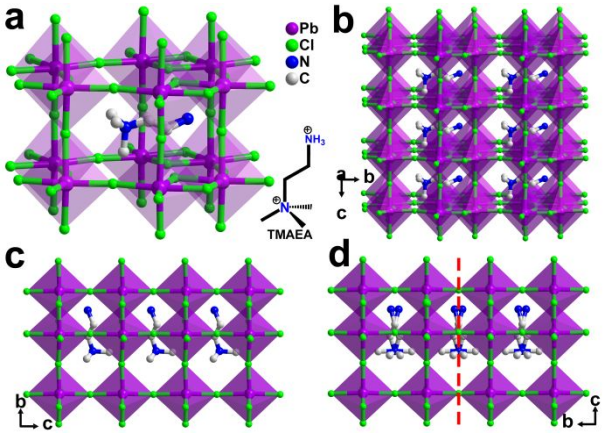

Figure 1. (a, b) 3D perovskite-related structure of $[TMAEA]Pb_2Cl_6$ at 293 K. (c) Packing view of the structure at 293 K. (d) Packing view of the structure at 423 K. The red dash line denotes a mirror plane.

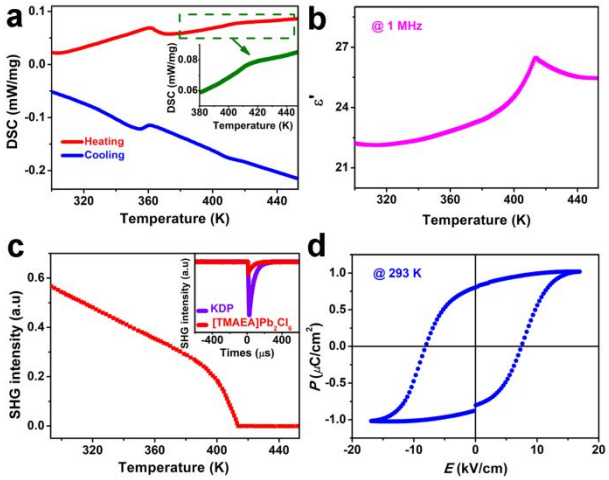

Figure 2. Ferroelectric and related properties of $[TMAEA]Pb_2Cl_6$. (a) DSC curves. (b) Temperature-dependent ε' at 1 MHz in the heating run. (c) Temperature-dependent SHG intensity. Inset: SHG intensity of $[TMAEA]Pb_2Cl_6$ and KDP at 293 K. (d) *P*–*E* hysteresis loop recorded at 293 K.

The phase transition of $[TMAEA]Pb_2Cl_6$ at T_2 is the *mmm*F*mm*2 type ferroelectric one,[18] accompanied by the symmetry breaking of 8 symmetry elements (E, $2\sigma_v$, i, σ_h, $2C_2'$, and C_2) in *mmm* (D_{2h}) point group decreasing to 4 symmetry elements (E, $2\sigma_v$, and C_2) in *mm*2 (C_{2v}) point group. The Curie temperature of $[TMAEA]Pb_2Cl_6$ (T_2, 412 K) is higher than those of most of molecular ferroelectrics including the lead halide ones,[8] such as $[(CH_3)_3NCH_2I]PbI_3$ (312 K),[13a] [cyclohexylammonium]$_2PbBr_4$ (363 K),[7b] and [4,4-diflorocyclohexylammonium]$_2PbI_4$ (377 K),[13b] and even higher than the 393 K of inorganic perovskite ferroelectric $BaTiO_3$. We then confirm that $[TMAEA]Pb_2Cl_6$ is a ferroelectric by the observation of a typical polarization−electric field (*P*–*E*) hysteresis loop at 293 K (Figure 2d). The saturate spontaneous polarization value of $[TMAEA]Pb_2Cl_6$ is about 1 $\mu C/cm^2$, which is larger than those of the first molecular ferroelectric Rochelle salt (0.25 $\mu C/cm^2$),[8] the molecular perovskite $[NMe_4]CdBr_3$ (0.12 $\mu C/cm^2$),[19a] and the recently discovered anti-perovskite $[(CH_3)_3NH]_3(MnBr_3)(MnBr_4)$ (0.45 $\mu C/cm^2$).[19b]

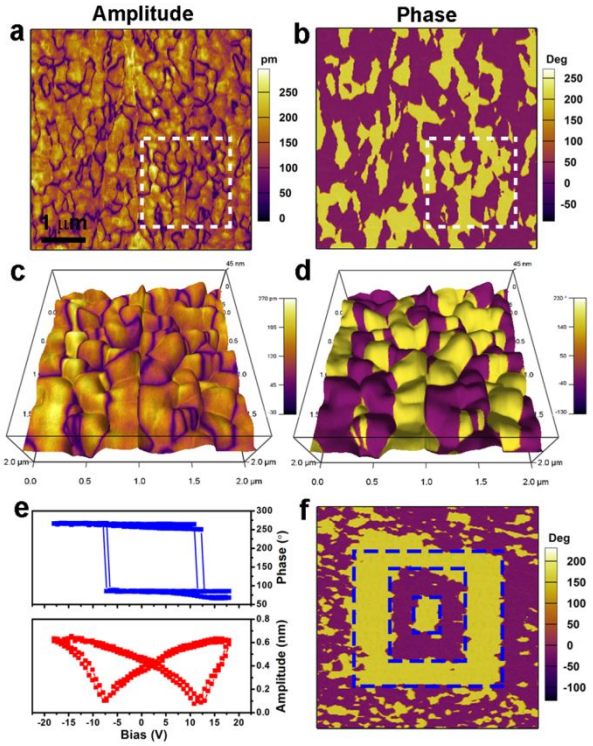

Figure 3. Domain structure and polarization switching for $[TMAEA]Pb_2Cl_6$. (a) Lateral PFM amplitude and (b) phase images for a region of 5 × 5 m. (c, d) Lateral PFM amplitude and phase of the region marked by white dashed box in a and b overlaid on the 3D topographic image, respectively. (e) Measured PFM switching spectroscopy on an arbitrary point of the thin film. (f) Box-in-box domain pattern created by three steps electric poling.

Further, we performed Piezoresponse Force Microscopy (PFM) measurements to examine the ferroelectricity of $[TMAEA]Pb_2Cl_6$ in its thin film samples. The lateral PFM imaging shows that the shape of the spontaneous domains is highly irregular. An example was shown in Figure 3a and b. Domain walls can be clearly observed in the amplitude image and the phase contrasts between the adjacent domains are 180˚. The vertical PFM imaging for this region shows weak amplitude response and blurry phase contrast (Figure S6b and c), indicating the polarization of this region predominantly lies in the in-plane direction. It is clearly show the domain pattern appears to be closely related to the grain structure of the thin film (topographic image see Figure S6a). Hence, to exclude the issue that the PFM contrast comes from the topography, we overlaid the PFM images on the 3D topographic image. As shown in Figure 3c and d, the 3D images demonstrate that the domain structure have no correlation with the morphology.

Next, we carried out polarization switching tests by PFM. Firstly, the PFM switching spectroscopy on a single point of the thin film was obtained. The hysteretic phase loops and typical butterfly shape of amplitude loops evidence the robust ferroelectric polarization in $[TMAEA]Pb_2Cl_6$ (Figure 3e). Regard to a larger region of polarization switching, we write the domains in the central region of a selected region with three steps electric poling. Finally, a box-in-box domain pattern was created (Figure 3f), further confirming the switchable polarization in $[TMAEA]Pb_2Cl_6$. Detailed description of the switching experiments refers to Figure S7.

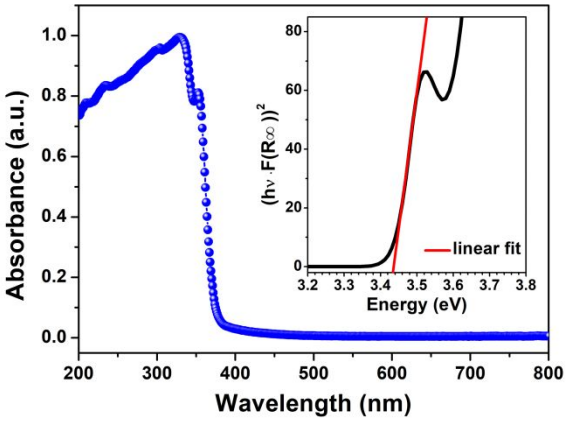

Figure 4. UV-vis absorption spectra of $[TMAEA]Pb_2Cl_6$.

Ultraviolet-visible (UV-vis) absorption spectra of $[TMAEA]Pb_2Cl_6$ shows a sharp absorption in the UV region at around 370 nm (Figure 4), indicating the direct bandgap semiconductor nature, which is commonly seen in lead halide perovskite.[2,7] The Tauc plot reveals a bandgap of approximately 3.43 eV, which is slightly smaller than that (3.65 eV) of the 2D lead-chloride perovskite ferroelectric $(benzylammonium)_2PbCl_4$,[7a] while slightly larger than that (3.16 eV) of the 3D lead-chloride perovskite $[CH_3NH_3]PbCl_3$.[20]

In conclusion, we presented a 3D lead halide perovskite-related ferroelectric $[TMAEA]Pb_2Cl_6$, which contains a unique 3D lead-chloride framework of both corner-sharing and edge-sharing $PbCl_6$ octahedral. $[TMAEA]Pb_2Cl_6$ shows a ferroelectric phase transition at the high Curie temperature of 412 K and a clear ferroelectricity at room temperature with a spontaneous polarization of 1 $\mu C/cm^2$. $[TMAEA]Pb_2Cl_6$ also possesses semiconducting property with a direct bandgap of 3.43 eV. As the first example of 3D lead halide ferroelectric showing a clear ferroelectricity, the finding of $[TMAEA]Pb_2Cl_6$ throws light on the exploration of more excellent 3D lead halide ferroelectrics with tremendous application potential.

ASSOCIATED CONTENT

Supporting Information

The Supporting Information is available free of charge on the ACS Publications website.
Experimental details, supporting figures S1−S7, supporting Tables S1 and S2, and X-ray crystallographic data (CIF) for this article.

Corresponding Author

*xiongrg@seu.edu.cn

Notes

The authors declare no competing financial interest.

ACKNOWLEDGMENT

This work was supported by the National Natural Science Foundation of China (21991142, 21831004 and 21427801).

REFERENCES

(1) (a) Jena, A. K.; Kulkarni, A.; Miyasaka, T. Halide Perovskite Photovoltaics: Background, Status, and Future Prospects. *Chem. Rev.* **2019**, *119*, 3036−3103; (b) Lin, J.; Lai, M.; Dou, L.; Kley, C. S.; Chen, H.; Peng, F.; Sun, J.; Lu, D.; Hawks, S. A.; Xie, C.; Cui, F.; Alivisatos, A.

P.; Limmer, D. T.; Yang, P. Thermochromic Halide Perovskite Solar Cells. *Nat. Mater.* **2018**, *17*, 261−267; (c) Veldhuis, S. A.; Boix, P. P.; Yantara, N.; Li, M. J.; Sum, T. C.; Mathews, N.; Mhaisalkar, S. G. Perovskite Materials for Light Emitting Diodes and Lasers. *Adv. Mater.* **2016**, *28*, 6804−6834; (d) Stoumpos, C. C.; Kanatzidis, M. G. Halide Perovskites: Poor Man's High-Performance Semiconductors. *Adv. Mater.* **2016**, *28*, 5778−5793; (e) Dou, L.; Wong, A. B.; Yu, Y.; Lai, M.; Kornienko, N.; Eaton, S. W.; Fu, A.; Bischak, C. G.; Ma, J.; Ding, T.; Ginsberg, N. S.; Wang, L.-W.; Alivisatos, A. P.; Yang, P. Atomically Thin Two-Dimensional Organic-Inorganic Hybrid Perovskites. *Science* **2015**, *349*, 1518−1521; (f) Liu, Y.; Siron, M.; Lu, D.; Yang, J.; dos Reis, R.; Cui, F.; Gao, M.; Lai, M.; Lin, J.; Kong, Q.; Lei, T.; Kang, J.; Jin, J.; Ciston, J.; Yang, P. Self-Assembly of Two-Dimensional Perovskite Nanosheet Building Blocks into Ordered Ruddlesden−Popper Perovskite Phase. *J. Am. Chem. Soc.* **2019**, *141*, 13028−13032.

(2) (a) Manser, J. S.; Christmas, J. A.; Kamat, P. V. Intriguing Optoelectronic Properties of Metal Halide Perovskites. *Chem. Rev.* **2016**, *116*, 12956−13008; (b) Lee, M. M.; Teuscher, J.; Miyasaka, T.; Murakami, T. N.; Snaith, H. J. Efficient Hybrid Solar Cells Based on Meso-Superstructured Organometal Halide Perovskites. *Science* **2012**, *338*, 643−647; (c) Stoumpos, C. C.; Malliakas, C. D.; Kanatzidis, M. G. Semiconducting tin and lead iodide perovskites with organic cations: phase transitions, high mobilities, and near-infrared photoluminescent properties. *Inorg. Chem.* **2013**, *52*, 9019−9038.

(3) Saparov, B.; Mitzi, D. B. Organic-inorganic perovskites: structural versatility for functional materials design. *Chem. Rev.* **2016**, *116*, 4558−4596.

(4) Kieslich, G.; Sun, S.; Cheetham, A. K. An Extended Tolerance Factor Approach for Organic-Inorganic Perovskites. *Chem. Sci.* **2015**, *6*, 3430−3433.

(5) (a) Mao, L.; Stoumpos, C. C.; Kanatzidis, M. G. Two-dimensional hybrid halide perovskites: principles and promises. *J. Am. Chem. Soc.* **2019**, *141*, 1171−1190; (b) Spanopoulos, I.; Ke, W.; Stoumpos, C. C.; Schueller, E. C.; Kontsevoi, O. Y.; Seshadri, R.; Kanatzidis, M. G. Unraveling the Chemical Nature of the 3D "Hollow" Hybrid Halide Perovskites. *J. Am. Chem. Soc.* **2018**, *140*, 5728−5742; (c) Mao, L.; Wu, Y.; Stoumpos, C. C.; Wasielewski, M. R.; Kanatzidis, M. G. White-light emission and structural distortion in new corrugated two-dimensional lead bromide perovskites. *J. Am. Chem. Soc.* **2017**, *139*, 5210−5215.

(6) (a) Li, W.; Wang, Z.; Deschler, F.; Gao, S.; Friend, R. H.; Cheetham, A. K. Chemically Diverse and Multifunctional Hybrid Organic-Inorganic Perovskites. *Nat. Rev. Mater.* **2017**, *2*, 16099; (b) Mitzi, D. B. Synthesis, Structure and Properties of Organic-Inorganic Perovskites and Related Materials. *Prog. Inorg. Chem.* **1999**, *48*, 1−121.

(7) (a) Liao, W. Q.; Zhang, Y.; Hu, C. L.; Mao, J. G.; Ye, H. Y.; Li, P. F.; Huang, S. D.; Xiong, R. G. A lead-halide perovskite molecular ferroelectric semiconductor. *Nat. Commun.* **2015**, *6*, 7338; (b) Ye, H. Y.; Liao, W. Q.; Hu, C. L.; Zhang, Y.; You, Y. M.; Mao, J. G.; Xiong, R. G. Bandgap engineering of lead-halide perovskite-type ferroelectrics. *Adv. Mater.* **2016**, *28*, 2579−2586.

(8) Zhang, W.; Xiong, R.-G. Ferroelectric Metal−Organic Frameworks. *Chem. Rev.* **2012**, *112*, 1163−1195.

(9) Yuan, Y.; Xiao, Z.; Yang, B.; Huang, J. Arising Applications of Ferroelectric Materials in Photovoltaic Devices. *J. Mater. Chem. A* **2014**, *2*, 6027−6041.

(10) (a) Choi, T.; Lee, S.; Choi, Y. J.; Kiryukhin, V.; Cheong, S.-W. Switchable Ferroelectric Diode and Photovoltaic Effect in $BiFeO_3$. *Science* **2009**, *324*, 63−66; (b) Yang, S. Y.; Seidel, J.; Byrnes, S. J.; Shafer, P.; Yang, C.-H.; Rossell, M. D.; Yu, P.; Chu, Y.-H.; Scott, J. F.; Ager, J. W.; Martin, L. W.; Ramesh, R. Above-bandgap voltage from ferroelectric photovoltaic devices. *Nat. Nanotechnol.* **2010**, *5*, 143−147.

(11) (a) Rossi, D.; Pecchia, A.; der Maura, M. A.; Leonhard, T.; Rohm, H.; Hoffmann, M. J.; Colsmann, A.; Di Carlo, A. On the Importance of Ferroelectric Domains for the Performance of Perovskite Solar Cells. *Nano Energy* **2018**, *48*, 20−26; (b) Bi, F.; Markov, S.; Wang, R.; Kwok, Y.; Zhou, W.; Liu, L.; Zheng, X.; Chen, G.; Yam, C. Enhanced Photovoltaic Properties Induced by Ferroelectric Domain Structures in Organometallic Halide Perovskites. *J. Phys. Chem. C* **2017**, *121*, 11151−11158; (c) Kutes, Y.; Ye, L.; Zhou, Y.; Pang, S.; Huey, B. D.; Padture, N. P. Direct Observation of Ferroelectric Domains in Solution-Processed $CH_3NH_3PbI_3$ Perovskite Thin Films. *J. Phys. Chem. Lett.* **2014**, *5*, 3335−3339.

(12) (a) Li, L.; Liu, X.; Li, Y.; Xu, Z.; Wu, Z.; Han, S.; Tao, K.; Hong, M.; Luo, J.; Sun, Z. Two-Dimensional Hybrid Perovskite-Type Ferroelectric for Highly Polarization-Sensitive Shortwave Photodetection. *J. Am. Chem. Soc.* **2019**, *141*, 2623−2629; (b) Li, L. N.; Shang, X. Y.; Wang, S. S.; Dong, N. N.; Ji, C. M.; Chen, X. Y.; Zhao, S. G.; Wang, J.; Sun, Z. H.; Hong, M. C.; Luo, J. H. Bilayered Hybrid Perovskite Ferroelectric with Giant Two-Photon Absorption. *J. Am. Chem. Soc.* **2018**, *140*, 6806−6809.

(13) (a) Hua, X. N.; Liao, W. Q.; Tang, Y. Y.; Li, P. F.; Shi, P. P.; Zhao, D.; Xiong, R. G. A Room-Temperature Hybrid Lead Iodide Perovskite Ferroelectric. *J. Am. Chem. Soc.* **2018**, *140*, 12296−12302; (b) Sha, T.-T.; Xiong, Y.-A.; Pan, Q.; Chen, X.-G.; Song, X.-J.; Yao, J.; Miao, S.-R.; Jing, Z.-Y.; Feng, Z.-J.; You, Y.-M.; Xiong, R.-G. Fluorinated 2D Lead Iodide Perovskite Ferroelectrics. *Adv. Mater.* **2019**, *31*, 1901843; (c) Shi, P.-P.; Lu, S.-Q.; Song, X.-J.; Chen, X.-G.; Liao, W.-Q.; Li, P.- F.; Tang, Y.-Y.; Xiong, R.-G. Two-Dimensional Organic-Inorganic Perovskite Ferroelectric Semiconductors with Fluorinated Aromatic Spacers. *J. Am. Chem. Soc.* **2019**, *141*, 18334−18340; (d) Wang, S.; Liu, X.; Li, L.; Ji, C.; Sun, Z.; Wu, Z.; Hong, M.; Luo, J. An Unprecedented Biaxial Trilayered Hybrid Perovskite Ferroelectric with Directionally-Tunable Photovoltaic Effects. *J. Am. Chem. Soc.* **2019**, *141*, 7693−7697; (e) Chen, X.-G.; Song, X.-J.; Zhang, Z.-X.; Li, P.-F.; Ge, J.-Z.; Tang, Y.-Y.; Gao, J.-X.; Zhang, W.-Y.; Fu, D.-W.; You, Y.-M.; Xiong, R.-G. Two-Dimensional Layered Perovskite Ferroelectric with Giant Piezoelectric Voltage Coefficient. *J. Am. Chem. Soc.* **2020**, *142*, 1077−1082; (f) Yang, C. K.; Chen, W. N.; Ding, Y. T.; Wang, J.; Rao, Y.; Liao, W. Q.; Tang, Y. Y.; Li, P. F.; Wang, Z. X.; Xiong, R. G. The First 2D Homochiral Lead Iodide Perovskite Ferroelectrics: [*R*- and *S*-1-(4-Chlorophenyl)ethylammonium]$_2$PbI$_4$. *Adv. Mater.* **2019**, *31*, 1808088; (g) Wu, Z. Y.; Ji, C. M.; Li, L. N.; Kong, J. T.; Sun, Z. H.; Zhao, S. G.; Wang, S. S.; Hong, M. C.; Luo, J. H. Alloying *n*-Butylamine into $CsPbBr_3$ To Give a Two-Dimensional Bilayered Perovskite Ferroelectric Material. *Angew. Chem. Int. Ed.* **2018**, *57*, 8140−8143.

(14) (a) Strelcov, E.; Dong, Q.; Li, T.; Chae, J.; Shao, Y.; Deng, Y.; Gruverman, A.; Huang, J.; Centrone, A. $CH_3NH_3PbI_3$ perovskites: Ferroelasticity revealed. *Sci. Adv.* **2017**, *3*, e1602165; (b) Xiao, Z.; Yuan, Y.; Shao, Y.; Wang, Q.; Dong, Q.; Bi, C.; Sharma, P.; Gruverman, A.; Huang, J. Giant Switchable Photovoltaic Effect in Organometal Trihalide Perovskite Devices. *Nat. Mater.* 2015, 14, 193−198; (c) Rakita, Y.; Bar-Elli, O.; Meirzadeh, E.; Kaslasi, H.; Peleg, Y.; Hodes, G.; Lubomirsky, I.; Oron, D.; Ehre, D.; Cahen, D. Tetragonal $CH_3NH_3PbI_3$ is ferroelectric. *Proc. Natl. Acad. Sci. U. S. A.* **2017**, *114*, E5504.

(15) Poglitsch, A.; Weber, D. Dynamic Disorder in Methylammoniumtrihalogenoplumbates (II) Observed by Millimeter-Wave Spectroscopy. *J. Chem. Phys.* **1987**, *87*, 6373−6378.

(16) (a) Xu, G. C.; Zhang, W.; Ma, X. M.; Chen, Y. H.; Zhang, L.; Cai, H. L.; Wang, Z. M.; Xiong, R. G.; Gao, S. Coexistence of magnetic and electric orderings in the metal-formate frameworks of $[NH_4][M(HCOO)_3]$. *J. Am. Chem. Soc.* **2011**, *133*, 14948−14951; (b) Xu, G.-C.; Ma, X.-M.; Zhang, L.; Wang, Z.-M.; Gao, S. Disorder−order ferroelectric transition in the metal formate framework of $[NH_4][Zn(HCOO)_3]$. *J. Am. Chem. Soc.* **2010**, *132*, 9588−9590; (c) Pan, Q.; Liu, Z.-B.; Tang, Y.-Y.; Li, P.-F.; Ma, R.-W.; Wei, R.-Y.; Zhang, Y.; You, Y.-M.; Ye, H.-Y.; Xiong, R.-G. A Three-Dimensional Molecular Perovskite Ferroelectric: (3-Ammoniopyrrolidinium)$RbBr_3$. *J. Am. Chem. Soc.* **2017**, *139*, 3954−3957; (d) Ye, H.-Y.; Tang, Y.-Y.; Li, P.-F.; Liao, W.-Q.; Gao, J.-X.; Hua, X.-N.; Cai, H.; Shi, P.-P.; You, Y.-M.; Xiong, R.-G. Metal-free three-dimensional perovskite ferroelectrics. *Science* **2018**, *361*, 151−155.

(17) Mao, L.; Guo, P.; Kepenekian, M.; Hadar, I.; Katan, C.; Even, J.; Schaller, R. D.; Stoumpos, C. C.; Kanatzidis, M. G. Structural Diversity in White-Light-Emitting Hybrid Lead Bromide Perovskites. *J. Am. Chem. Soc.* **2018**, *140*, 13078−13088.

(18) Aizu, K. Possible species of "ferroelastic" crystals and of simultaneously ferroelectric and ferroelastic crystals. *J. Phys. Soc. Jpn.* **1969**, *27*, 387−396.

(19) (a) Gesi, K. Ferroelectricity in $N(CH_3)_4CdBr_3$. *J. Phys. Soc. Jpn.* **1990**, *59*, 432−434; (b) Wei, Z.; Liao, W.-Q.; Tang, Y.-Y.; Li, P.-F.; Shi, P.-P.; Cai, H.; Xiong, R.-G. Discovery of an Antiperovskite Ferroelectric in $[(CH_3)_3NH]_3(MnBr_3)(MnBr_4)$. *J. Am. Chem. Soc.* **2018**, *140*, 8110−8113.

(20) Kumawat, N. K.; Dey, A.; Kumar, A.; Gopinathan, S. P.; Narasimhan, K. L.; Kabra, D. Band Gap Tuning of $CH_3NH_3Pb(Br_{1-x}Cl_x)_3$ Hybrid Perovskite for Blue Electroluminescence. *ACS Appl. Mater. Interfaces* **2015**, *7*, 13119−13124.

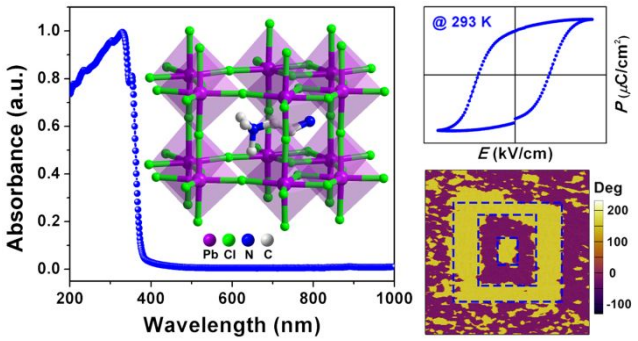
Absorbance (a.u.)
Wavelength (nm)
Pb Cl N C
@ 293 K
P (μC/cm²)
E (kV/cm)
Deg
200
100
0
-100